Journal of Materials Chemistry B

Accepted Manuscript

ROYAL SOCIETY OF CHEMISTRY

www.rsc.org/materialsB

Self-Assembled Zein-Sodium Carboxymethyl Cellulose Nanoparticles as Effective Drug Carrier and Transporter

Hongshan Liang[a,b], *Qingrong Huang*[c], *Bin Zhou*[a,b], *Lei He*[a,b], *Liufeng Lin*[a,b], , *Yaping An*[a,b], *Yan Li*[a,b], *Shilin Liu*[a,b], *Yijie Chen*[a,b], *Bin Li*[a,b]*

[a] College of Food Science and Technology, Huazhong Agricultural University, Wuhan 430070, China

[b] Key Laboratory of Environment Correlative Dietology (Huazhong Agricultural University), Ministry of Education

[c] Department of Food Science, Rutgers, The State University of New Jersey, 65 Dudley Rd, New Brunswick, NJ 08901, USA

*Corresponding author: Telephone: +86-27-63730040; Fax: +86-27-87282966

E-mail address: libinfood@mail.hzau.edu.cn

Abstract

In this work, biodegradable nanoparticles (NPs) were assembled with sodium carboxymethyl cellulose (CMC) and zein to produce zein-CMC NPs. Paclitaxel (PTX) was 95.5% encapsulated at a zein-CMC weight ratio of 1:3 and the NPs were spherical with an average particle size of approximately 159.4 nm, with the PTX concentration maintained at 80 μg ml^{-1}. The NPs demonstrated good stability at broad range of pH values ranging from 3.7 to 11.0. The Zein-CMC NPs were seen to provide a sustained release of PTX for up to 72 h, which led to an 80% release of the total loaded PTX in vitro. Confocal laser scanning microscopy (CLSM) and flow cytometry studies showed that the zein-CMC NPs could effectively transport encapsulated molecules into both drug-sensitive (HepG2 cells) and drug-resistant cancer cells (MCF-7 cells). Moreover, in vitro viability studies revealed that the PTX-loaded zein-CMC NPs had greater potency than free PTX in the PTX resistant MCF-7 cells at higher concentration. Furthermore, PTX-loaded NPs displayed obvious efficiency in the apoptosis of HepG2 cells. Zein-CMC NPs showed significant potential as a highly versatile and potent platform for cancer therapy.

Keywords: Nanoparticles, paclitaxel, cellular-uptake, cytotoxicity

1. Introduction

Paclitaxel (PTX), one of the best anti-neoplastic agents, has been approved to effectively kill a wide variety of tumor cells[1, 2]. Although it is therapeutically very effective, it has significantly limited the clinical application in its natural form due to its poor solubility in water. One commercial preparation of PTX is Taxol®, a concentrated solution composed of a 1:1 blend of Cremophor®EL (polyoxyethylated castor oil) and dehydrated ethanol. However, the presence of Cremophor®EL is reported to be responsible for nephrotoxicity, neurotoxicity and hypersensitivity[3]. Therefore, to minimize the side effects of the formulation, several drug delivery systems, such as microspheres[4], polymeric micelles[5,6], liposomes[7-10] and nanoparticles (NPs)[11-13] were proposed. Among these strategies, NPs have shown great potential as carriers with decreased side effects and enhanced tumor delivery[14,15].

NPs are known to penetrate disorganized and unsealed tumor vasculature and then accumulate in certain solid tumors through enhanced permeability and retention (EPR) to provide a unique phenomenon of solid tumors with anatomical and pathophysiological differences from normal tissues[16,17]. Although numerous inorganic and metal NPs, such as silica[18], gold[19] and silver[20] have been developed as potential diagnostic and therapeutic drug delivery agents for biomedical application, they tend to accumulate in the organs and tissues and thus have potential cytotoxic effects [21]. To avoid potential cytotoxicity, the NPs utilized in drug delivery are required to be biocompatible and fully metabolized after degradation in the body [22,23].

In recent years, self-assembled biodegradable NPs from natural polymers have

attracted considerable attention as potential drug delivery vehicles. Protein-based polymers, such as albumin[24], gelatin[25] and milk protein[26], represent a major class of biomaterials for the development of NPs utilized in encapsulation due to their enhanced properties of absorbability and low toxicity in the degradation of end products[27,28]. However, they also face limitations due to rapid solubilization in aqueous environments and thus have rapid drug release profiles. As an alcohol-soluble protein obtained from corn, zein has attracted widespread interest in drug delivery systems due to its intrinsic excellent biocompatibility and biodegradability[29]. Zein has been extensively investigated in the encapsulation of bioactive compounds because of its capability to form self-assembled NPs and more importantly, its capability for sustained drug release. It has thus been utilized in food and pharmaceutical applications, such as heparin[30], gitoxin[31], fish oil[32], and curcumin[33], etc. However, in many instances, the resultant zein NPs can be rapidly taken up by macrophagesprotein due to their protein origins and hydrophobicity, resulting in strong immunogenicity[34,35]. It was proposed that the enhanced bioefficacy by NPs could be achieved through the surface coating of zein NPs with a second layer of hydrophilic polysaccharide for an optimized balance of hydrophobic and hydrophilic elements[36,37]. Sodium carboxymethyl cellulose (CMC), a cellulose derivative, has been considered to be a versatile polymer for encapsulation and delivery of active ingredients. Due to its attractive functional properties and widespread availability[38,39], CMC is an interesting candidate for the protection of coated zein NPs. Although there are numerous previous reports of the synthesis of zein NPs, there remain needs for the

study of cellular uptake in zein-based delivery systems.

In this article, a PTX-loaded zein-CMC NPs delivery system was developed using a liquid−liquid phase separation approach. Optimized preparation, characterization and release behavior was achieved in the PTX drug, and cell viability was evaluated against drug-sensitive (HeLa and HepG2 cells) and drug-resistant cancer cells (MCF-7 and A549 cells). Using coumarin-6 as the fluorescence probe, the cellular uptake of the NPs was investigated. Furthermore, the apoptosis of both drug-sensitive and drug-resistant cancer cells was examined under the treatment of various formulations by flow cytometry. Indirect immunofluorescence staining was then performed for the observation of microtubule dynamic instability in both drug-sensitive and drug-resistant cancer cells after incubation with either free PTX or PTX-loaded NPs.

2. Materials and methods

2.1. Materials

Zein (Z0001) was purchased from Tokyo Chemical Industry, Co.,Ltd. (Tokyo, Japan). Paclitaxel (PTX) was supplied by Nanjing Zelang Pharm Co.,Ltd (Nanjing, China). Sodium carboxymethyl cellulose (CMC, degree of substitution, 0.7; Mw=90kDa) were purchased from Sinopharm Chemical Reagent Co., Ltd (Shanghai, China). Coumarin-6, DAPI (4,6-diamidino-2-phenylindole) and LysoTracker Red were purchased from Invitrogen (USA). Cremophor®EL, phosphate buffer solution (PBS) amd MTT [3-(4, 5-dimethylthiazol-2-yl)-2,5-diphenyl tetrazolium bromide] were purchased from Sigma-Aldrich (St. Louis, MO, USA). Dubelcco's modified Eagle's

medium (DMEM), Eagle's minimum essential medium (MEM), fetal bovine serum (FBS), trypsin–EDTA and penicillin–streptomycin mixtures were from Gibco®BRL (Carlsbad, CA, USA). Methanol and acetonitrile were of HPLC-grade. Ultrapure water (18.2 MΩ, Milli-Q Ultrapure Water System) was utilized throughout all experiments.

2.2. Preparation of zein-CMC nanoparticles

Zein was dissolved in aqueous ethanol solutions (75% v/v) to obtain a stock solution with a final concentration of 5mg ml^{-1}. CMC solution was prepared by dissolving weighed CMC powder into water. Then, the above zein solution was rapidly mixed with CMC solution. The solution was under vigorous stirring until a single phase was formed. Solutions consisting of different weight ratios of zein:CMC at 2:1, 1:1,1:2,1:3 and 1:4, respectively, were prepared.

PTX (5 mg mL^{-1}) was dissolved in pure ethanol as a stock solution. Different volume of PTX solution was dropwise added into zein solution under mild stirring for 60 min in a 25ml glass vial. The formulation containing PTX was prepared by pouring zein-PTX solution into CMC solution (containing Tween80), under vigorous stirring until a permanent light-blue color was maintained, resulting in different weight ratios of zein:CMC at 2:1, 1:1, 1:2, 1:3 and 1:4, respectively. The final concentration of Tween80 was 0.2%.

2.3. Characterizations of NPs

2.3.1. Particle size and zeta potential measurements

Dynamic laser scattering (DLS) and zeta potential measurements of all blank and

PTX-loaded NPs were performed on a commercial laser light scattering instrument (Malvern ZEN3690, Malvern Instruments) at 25□and 90°scattering angle.

2.3.2 Morphology observation

The surface morphology of nanoparticles was observed by the field emission scanning electron microscope (FE-SEM, S-4800, Hitachi Ltd., Japan). Transmission electron microscopic (TEM) images were taken on a JEM-2100F (JEOL, Japan). The chemical structures of preparation ingredients (zein, CMC and PTX) and NPs (NPs and PTX-loaded NPs) were monitored by FTIR of Jasco 4100 series with an attenuated total reflection cell (Jasco Inc., Easton, MO). X-ray diffraction patterns were acquired at room temperature on a Bruker D8-Advance Diffractometer (Bruker AXS Inc., Madison,WI, USA) with backgroundless sample holders. The data were collected over an angular range from 5°to 50° 2θ in continuous mode using a step size of 0.02° 2θ and step time of 5 seconds.

2.4. Encapsulation efficiency (EE) and loading capacity (LC)

The collected sample was ultracentrifuged at 4000×g for 30 min in a refrigerated centrifuge (TGL-20000cR) with angle rotor[40]. Then, the released PTX in the supernatant was determined by high-performance liquid chromatography (HPLC). The HPLC system (LC-2010C, Shimadzu, Japan) was equipped with a Lichrospher C18 column (4.6×250 mm, 5μm) with a mobile phase of methanol, purified water and acetonitrile (v/v/v=23:41:46). The flow rate and column temperature were set at 1 ml min^{-1} and 30 ℃, respectively. Total run time was 45 min for each sample. PTX was detected at a wavelength of 227 nm. The encapsulation efficiency (EE, %) and the

drug loading capacity (LC, %) were calculated based on the following equations:

EE (%) = weight of PTX in NPs/weight of the feeding PTX ×100%

LC (%) = weight of PTX in NPs/weight of the feeding NPs ×100%

2.5. In vitro PTX release

In order to determine the drug release profile, 5mL PTX-loaded NPs (PTX concentration, 80μg mL^{-1}) or free PTX (80μg mL^{-1}) was placed in a dialysis bag (molecular weight cutoff 8–14 kDa, Millipore, USA), which was then dialyzed against 50 mL phosphate buffer solution (PBS, pH 7.4 with 0.2% Tween-80 to provide sink condition). The experiment was carried out under the water bath at 37□ with shaken speed of 100 rpm. At each predetermined time interval, 1 mL of PBS buffer solution containing released PTX was taken out from each vial, and equal volumes of respective fresh buffer solution were replenished[41]. The amount of PTX in the release medium was determined by HPLC.

Released (%) =Released PTX /Total amount of PTX entrapped inside the NPs×100%

2.6. Cell culture

Human cervical carcinoma HeLa cells and human hepatocellular carcinoma HepG2 cells were cultured in DMEM, while human breast adenocarcinoma MCF-7 cells and human non-small-cell lung carcinoma A549 cells were cultured in MEM, supplemented with 10% fetal bovine serum and 1% penicillin–streptomycin at 37 □in humidified environment of 5% CO_2.

2.7. In vitro antitumor activity

HeLa, HepG2, MCF-7 and A549 cells were seeded in 96-well plates at the density of

1×10^4 cells per well and incubated for 24 h to allow cell attachment. After incubation, the medium was replaced by the fresh, antibiotic-free medium containing various NPs (either blank or PTX containing NPs) or PTX at concentrations ranging from 0.01 to 8μg mL^{-1} with further incubation for 24 and 48h. At designated time intervals, the medium was removed and the wells were washed with PBS for two times. 20μL MTT solution (0.5mg mL^{-1}) was then added to each well, and the plates were incubated for 4 h. The MTT-containing medium was then removed, and the resulting formazan crystals in the living cells were dissolved with DMSO (100μl). The absorbance of the formazan crystals at the absorption wavelengths of 490 nm were measured by using a microplate reader (Genios, Tecan, Mannedorf, Switzerland). Cell viability was calculated by using the following equation:

Cell viability (%) =Abs 490 nm of treated group/Abs 490 nm of control group×100%.

The toxicities of the PTX-loaded NPs and free PTX were also expressed as the inhibitory concentration at which 50% of cell growth inhibition was obtained (IC_{50}).

2.8. In vitro cellular uptake of NPs

To trace the cellular uptake of the NPs, the NPs were labeled with coumarin 6, and both quantitative and qualitative studies were carried out according to previous literature[42]. The zein solution containing 0.02% coumarin 6 (dissolved in 75% ethanol solution) was used in the preparation of fluorescent NPs with all other conditions remaining the same. Unreacted coumarin 6 was separated by centrifugation using ultrafilter.

HepG2 and MCF-7 cells were separately seeded in a 24-well plate at a density of

1×10^5 viable cells per well in 1 mL growth medium and the cells were incubated at 37 °C for 24 h to allow cell attachment. Then the culture medium was replaced by 1 mL of fresh medium containing coumarin 6-labeled PTX-NPs and incubated for 0.5, 2, 4, 6 or 12 h, respectively. Before observation, LysoTracker Red was added to the medium and cells were incubated for additional 1 h. Cells were washed with PBS and stained with 4′,6-diamidino-2-phenylindole (DAPI). Fluorescence images were collected using a confocal laser scanning microscopy (CLSM) (Zeiss LSM 710, Germany).

For quantitative study using flow cytometry, HepG2 and MCF-7 cells were seeded onto 6-well plates at a density of 1×10^5 viable cells per well, incubated for 24 h. Then the culture medium was replaced by fresh medium containing coumarin 6-labeled PTX-NPs and incubated for 0.5, 2, 4, 6 or 12 h, respectively. Cells without any treatment were used as the control. The cells were then washed with PBS and harvested. The cellular uptake of NPs was measured by using a Cytomics™ FC 500 flow cytometer (Beckman Coulter, Miami, FL, USA).

2.9. Apoptosis assay

HepG2 and MCF-7 cells were seeded in 6-well plates at the density of 5×10^5 cells per well, cultured for 24 h, and then incubated for 24 h with PTX, PTX-NPs and NPs, respectively, at the PTX concentration of 8μg mL^{-1} using drug-free culture medium as the negative control. At the end of the treatment, cells were harvested, washed with PBS, suspended in 500 mL binding buffer and stained by 5 mL Annexin V-FITC and 5 mL PI. The cells were incubated in the dark for 15 min and measured by using a

Cytomics™ FC500 flow cytometer (Beckman Coulter, Miami, FL, USA).

2.10. Immunofluorescence Staining of Tubulin Disruption

HepG2 and MCF-7 cells were seeded into 35 mm petri dish at a density of 5×10^5 cells per well and incubated overnight. Then the cultured cells were incubated with fresh medium containing free PTX or PTX-loaded NPs (HepG2, 1.0μg mL^{-1}; MCF-7, 8μg mL^{-1}) and incubated for 24 or 48 h. After the incubation, the cells were permeabilized with 0.1% Triton X-100 in PBS (pH 7.4) for 2 min and fixed with 4% paraformaldehyde in PBS (pH 7.4) at 30 min intervals, and blocked with 10% BSA for 30 min, followed by sequential incubation with mouse monoclonal antibody, and corresponding FITC coupled secondary antibody. The nuclei were stained with DAPI. Fluorescence images were collected by using a CLSM (Zeiss LSM 710, Germany).

2.11. Statistics analysis

Data are presented as the mean ± standard deviation. Statistical comparisons were analyzed by ANOVA analysis and Student's t-test. A value of $p < 0.05$ was considered to be significant.

3. Results and discussion

3.1. Optimization and Characterization of Zein-CMC NPs

Table 1 and Table S1 show the influence of zein and CMC ratios on the formation of NPs with and without PTX. The results indicated variation in the particle size depending on the molar ratio of zein to CMC. The smallest obtained particle size (135.3 nm) was achieved with ideal polydispersity (PDI) with a zein and CMC ratio of 1:3 (Table S1). The surface charge of the resulting NPs was

concentration-dependent and ranged from −50.4 to −58.3 mV, which provided greater colloidal stability and less toxicity for normal cells than positive charged NPs (Table S1). With the addition of PTX (50 μg ml^{-1}), the particle size and surface charge of NPs showed a slight change and the encapsulation efficiency (EE) reached 95.5% at a zein-CMC ratio of 1:3 (Table 1). Thus, the zein to CMC ratio in NPs was determined optimum at 1:3 and was used accordingly in the following experiments.

Figure S1 displayed the pH-responsiveness of NPs. With the exception of pH 2.6, the particle sizes and PDIs of zein-CMC NPs remained almost constant from pH 3.7 to 11.0. In addition, the charge of NPs was more negative than in CMC, which gradually increased between pH 2.6 and 5.8 and then stabilized at pH values above 5.8. The pH-response of NPs was linked to the molecular conformation of CMC under various pH values. At low pH values, most of the carboxyl groups in the CMC molecular chain were protonated in the form of −COOH, which may have led to a lower surface charge and larger particle size (Figure S1). With the increase of pH, the carboxyl groups gradually transformed into $-COO^-$ and the negative charge of NPs increased. Then, the particle size of the NPs decreased and became constant. In this work, the optimum stability of NPs was obtained at a broad range of pH values (3.7-11), which was advantageous for further application.

As shown in the FE-SEM images, the NPs were presented as solid and regular nanospheres (Figures 1a and 1b). The TEM images revealed that the NPs were dispersed as individual NPs with well-defined spherical shape and homogeneous distribution (Figure 1c). The addition of PTX did not instigate morphological changes

in the NPs (Figure 1e). Furthermore, the NPs solution (with and without PTX) remained light blue in color with good stability after 30 days of storage under 4 ºC. The particle size distribution maintained a mono-model structure and no shift was observed. Changes in the morphology of NPs were not observed (Figure 1d and f).

The FTIR spectra were shown in Figure S2. As shown, the amide I band of zein at 1640 cm^{-1} demonstrated a prominent C=O stretching, while the amide II band at 1533cm^{-1} demonstrated C-N stretching. The peaks of CMC at 1604cm^{-1} and 1419cm^{-1} were attributed to asymmetric and stretching vibrations of the −COO group. The spectral peaks in zein, CMC and zein-CMC NPs demonstrated shifts to 1621 cm^{-1}, 1545 cm^{-1} and 1417cm^{-1}, respectively. This indicated that there existed electrostatic bonding between zein and CMC[43]. In addition, the absorptions at 1742 cm^{-1} and 1070 cm^{-1} were attributed to PTX entrapped in the matrix of the zein-CMC NPs (Figure S2). Moreover, the hydrophobic qualities of both zein and PTX allowed hydrophobic interactions to contribute to the formation of the NPs. The XRD patterns of the NPs and pure PTX are shown in Figure S3. The major characteristic peaks of PTX were determined at 5.6°,9.1°,10.4°,12.7°and 21.1°, which was indicative of their highly crystalline nature[44]. In contrast, two smoother humps were observed in zein as opposed to previously obtained sharp peaks, demonstrating the amorphous nature of the protein[37]. The PTX specific peaks disappeared in all of the NPs, suggesting that the PTX in the NPs did not manifest in crystal form. This provided additional evidence for encapsulation.

3.2. Drug Encapsulation and Release Profiles

Figure 2 presents the encapsulation and release profiles of PTX in zein-CMC NPs. As shown in Figure 2a, the loading capacity (LC) increased with an initial increase in PTX concentration but corresponding decreases were also observed in EE. In addition, the particle size of NPs corresponded to the concentration of PTX. The smallest mean particle diameter (159.4 nm) was obtained at 80 μg ml^{-1}, with an increased concentration of PTX from 50μg ml^{-1} to 90μg ml^{-1}. In combination with the physical entrapment effect, PTX could interact with the hydrophobic microdomains of zein, resulting in a higher drug EE. A higher hydrophobic PTX content in the NPs was expected to increase the hydrophobic qualities of the NPs and increase the hydrophobic characteristics between the zein and PTX, resulting in closer integration and subsequent decreases in the particle size[33]. However, an increase in the PTX content 90μg ml^{-1} led to the increased precipitation on the particle surface of PTX, resulting in increased particle sizes.

The PTX-loaded zein-CMC NPs were 159.4 nm in size, which was highly suitable for anti-tumor drug delivery. This was consistent with previous reports that a particle size between 100 nm and 200 nm is optimal for the EPR effect and decreased blood clearance in tumor drug delivery[45,46]. Also the PTX-loaded NPs formulation system demonstrated strong potential for a practical drug delivery carrier with effective drug encapsulation capacity.

The in vitro release of PTX from the zein-CMC NPs was monitored in 0.01 M PBS with a pH of 7.4 at 37 ^{o}C (Figure 2b). Compared with bulk PTX, the zein-CMC NPs released PTX in a sustained manner, which provided enduring capacity in the fight

against cancer cells. After 10 h incubation, almost 100% of the PTX was solubilized from bulk PTX, while less than 40% was obtained from the NPs. About 80% of the PTX was released from NPs after 72 h incubation. In addition, a significant initial burst was not observed in the release curve. The controlled and sustained behavior of PTX could be attributed to the delay of water penetration as a result of the hydrophobic zein, thus inhibiting the diffusion of the drug into the release medium. The presence of CMC facilitated the formation of a second layer, providing a barrier against the diffusion of PTX and decreasing the rate of release. The relatively fast initial release was attributed to two factors. First, size was highly influential in the first release of PTX, as the small NPs had a much larger total surface area and there was a greater fraction of PTX near the surface, resulting in faster initial release. Second, the swelling of NPs instigated the release of any PTX that was not tightly wrapped into the solution. Under prolonged incubation time, the equilibrium swelling of NPs led to a very slow release stage. The PTX bound with zein-CMC NPs provided a very slow release rate via hydrophobic interaction.

3.3. Intracellular Uptake of PTX-Loaded NPs

The incorporation of small-molecular-weight drugs into the NPs altered the cellular and whole body pharmacokinetics of the drugs. In solid tumors, the EPR effect could facilitate the passive accumulation of nanomedicines in the tumor tissue[47]. Once in the extracellular space of tumors, nanomedicines are endocytosed by cells which appears to be the predominate mechanism of cellular internalization of the NPs and accumulate in intracellular organelles[48].

The cellular uptake of PTX-loaded NPs was evaluated on drug-sensitive HepG2 cells and drug-resistant MCF-7 cells at different time intervals using CLSM (Figure 3) and flow cytometry (Figure 4). The cancer cells were treated with coumarin 6-labeled NPs and then stained with LysoTracker Red and DAPI for the identification of lysosomes and the nucleus, respectively. As shown in Figure 3, the cells exhibited green coloring in the cytoplasm region with diffused distribution and blue fluorescence from the nucleus in DAPI, suggesting that the NPs had predominantly uniform distribution in the entire cell cytoplasm but not in the nucleus. In the HepG2 cells, minor green fluorescence could be observed at 30min, indicating limited endocytosis at this time (Figure 3a). At two hours post incubation, a marked increase in the fluorescence intensity could be observed in the cytoplasm (Figure 3a). In addition, the colocalization of green and red fluorescence was observed, revealing the transportation of some NPs to lysosomes. There was an obvious accumulation of NPs in lysosomes at 4 h (Figure 3a). In contrast with the HepG2 cells, only a few scattered fluorescence dots were observed in the cell cytoplasm of MCF-7 cells at 4 h, while fluorescence in the cell membranes was dramatically enhanced (Figure 3b). A schematic illustration for the formation of zein-CMC NPs with PTX and cellular-uptake behavior is shown in Scheme 1.

The results were quantitatively confirmed by flow cytometry measurements, which also revealed a consistent increase in the fluorescence intensity of HepG2 cells with increased incubation time from 0.5 to 12 h (Figures 4a and 4c). The coumarin-6 labeled NPs incubated for 0.5, 2, 4, 6 and 12h were obtained at cell percentages of

353 4.32, 86.82, 98.51, 98.56 and 98.68%, respectively. The cellular uptake of coumarin
354 6-labeled NPs peaked at 6 h and faded at 12h after incubation in MCF-7 cells, while
355 near equilibrium was achieved at 4h in HepG2 cells (Figure 4c). The intracellular
356 accumulation of coumarin 6-labeled NPs in MCF-7 cells were lower than in HepG2
357 cells. (Figure 4b and c: the coumarin-6 labeled NPs incubated for 0.5, 2, 4, 6 and 12h
358 were obtained with cell percentages of 14.55, 56.99, 62.35, 76.64 and 72.31,
359 respectively.)

360 **3.4. In vitro Cytotoxicity Study**

361 As the hydrophobic molecules were successfully transported into HepG2 and MCF-7
362 cells with the NPs, the in vitro dose- and time-dependent cytotoxicity was then
363 assayed against both the PTX sensitive (HeLa and HepG2) and PTX resistant (MCF-7
364 and A549) cancer cells. In Figure 5a-d, the in vitro cytotoxic effects of the NPs, free
365 PTX and PTX-loaded NPs are shown for the drug-sensitive cells (HepG2 and HeLa
366 cells). It was apparent that blank NPs did not show significant cytotoxicity. The
367 cytotoxic effect of PTX on the cells was dose- and time-dependent. Overall, the cell
368 viability reduced with increased PTX concentration and prolonged incubation time.
369 Notably, after 24 h incubation at the same PTX concentration, the cytotoxicity of the
370 encapsulated PTX was slightly lower than the bulk PTX in HeLa cells (Figure 5a).
371 The maximal half inhibitory concentrations (IC_{50}) were determined as 2.98 and 1.85
372 μg of PTX equiv mL^{-1} for PTX-NPs and free PTX, respectively (Table S2). However,
373 the cytotoxicity of encapsulated PTX was higher than the bulk PTX after 48 h
374 incubation with a PTX concentration of more than 1 □g mL^{-1} (Figure 5b). HepG2

cells showed increased sensitivity compared to the HeLa cells, in which lower IC_{50} values of 1.46 and 0.39 μg PTX equiv mL^{-1} were obtained after 24 h incubation for PTX-NPs and free PTX, respectively (Figure 5c and Table S2). The optimum cytotoxicity level for PTX-NPs and free PTX was obtained at 48 h incubation with the IC50 value at 0.38 and PTX at 0.02μg equiv mL^{-1} (Figure 5d). It should be noted that a reduction in the in vitro antitumor activity of PTX-loaded NPs after 24 h incubation was observed as the released drugs were structurally altered. The drug release process inside the tumor cells was further hindered by the hydrophobic nature of zein. As shown in Figure 2b, the drug release from the NPs after 24 h was determined as 54% of the total amount encapsulated in the NPs. Furthermore, the free PTX exhibited a stronger inhibition effect compared with the PTX-loaded NPs. This could be attributed to the quick transportation of the free drugs into the cells by passive diffusion due to the higher concentration gradient under in vitro conditions, which instantly affected cell growth devoid of the drug release process[49].

Figure 5e-h show the cell viability of the drug-resistant cells (MCF-7 and A549 cells) in the presence of NPs, free PTX and PTX-loaded NPs. As above, the pure NPs did not cause any reduction in cell viability. There was, however, an apparent difference between the cell death profiles of drug-sensitive cells and drug-resistant cells. After 24 h incubation, more than 70% of the cells were viable regardless of the bulk and encapsulated PTX concentrations. Higher concentrations of PTX were necessary to achieve effective cytotoxicity against PTX-resistant cells as compared to the PTX-sensitive tumor cells (Figure 5e-5h). Upon treatment with PTX-NPs, the cell

viabilities of MCF-7 cells were 73% at a PTX concentration of 8μg PTX equiv mL^{-1}. Nevertheless, PTX-NPs maintained their therapeutic effect against HepG2 cells by inducing similar toxicity at a PTX concentration of < 0.5μg PTX equiv mL^{-1}. Compared to free PTX, the PTX-loaded NPs contributed to a higher reduction in cell viability ($P<0.001$) for MCF-7 cells at a PTX concentration of 4μg and 8μg PTX equiv mL^{-1}. Breast cancer cells were characterized by a stromal microenvironment that consisted of highly abundant hyaluronan (HA), which could facilitate tumor progression by enhancing tumor growth, invasion and angiogenesis[50]. Furthermore, a high level of HA is the primary matrix determinant of drug barriers[51]. It was supposed that the application of small molecular-weight drugs into the cell interior would thus have significant impact. However, the PTX-loaded NPs could be more efficiently applied through the endocytose pathway for drug delivery into cells, which may have led to higher cytotoxic effects. This assumption was verified in the intracellular uptake experiments, which showed high fluorescence intensity in the cells.

3.5. In Vitro Apoptosis Assay

The influence of PTX formulations on cell death was further confirmed by apoptosis assay in $HepG_2$ cells and MCF-7 cells using flow cytometry. Figure 6a shows the apoptosis dot diagrams of HepG2 cells and MCF-7cells treated with the NPs, free PTX and PTX-loaded NPs. The percentage of HepG2 cells undergoing apoptosis significantly increased from 5.98% (control) to 21.37% and 18.06% after treatment with free PTX and PTX-NPs, respectively (Figure 6b). For resistant MCF-7 cells, cell apoptosis was also enhanced by the presence of PTX, as compared with the control

treatment (9.09%). Interestingly, the obtained apoptosis percentage in encapsulated PTX (20.01%) was higher than in bulk PTX (16.75%). These results indicated that apoptosis was induced by both PTX encapsulated in the NPs and released in the extracellular medium[52].

3.6. Effect of PTX-loaded NPs on Tubulin Polymerization

PTX is known to promote the polymerization of tubulin and result in the rearrangement of the cytoskeleton structure[53]. The disruption of the normal microtubule structure was examined using indirect immunofluorescence staining to observe the effects in both drug-sensitive and drug-resistant cancer cells after incubation with either free PTX or PTX-loaded NPs (Figure 7). Independent of the cell lines, the control cells without PTX treatments only demonstrated a limited amount of microtubules with long-distance organization. On the other hand, free PTX or PTX-loaded NPs treatment resulted in stabilized microtubules around the nuclei after 24 or 48 h of incubation in both the HepG2 and MCF-7 cells. Abnormal cell morphology was observed in some images as a result of cell death.

4. Conclusion

In this work, formulated drug-loaded zein-CMC NPs were first characterized and then assessed for their efficacy and suitability in drug delivery systems. The resultant PTX-loaded zein-CMC NPs were approximately 159.4 nm in diameter with a spherical shape and high encapsulation efficiency. In vitro studies of the drug release pattern showed a sustained release of PTX over a period of 72 h at a physiological pH. CLSM and flow cytometry studies showed that the PTX-loaded NPs had excellent

cellular uptake ability by both drug-sensitive HepG2 cells and drug-resistant MCF-7 cells. Cell viability assays indicated that the PTX-loaded NPs exhibited concentration- and time-dependent cytotoxicity. The flow cytometry assays indicated that the anticancer activity of the prepared PTX-NPs caused cell death via apoptosis. In these preliminary studies, zein-CMC NPs showed significant potential for application as cancer drug delivery vehicles.

Acknowledgements

This work was financially supported by the National Natural Science Foundation of China (No. 31071607). The authors would like to express their sincere gratitude to many conveniences offered by colleagues of Key Laboratory of Environment Correlative Dietology of Huazhong Agricultural University.

References

1. Z. G. Yue, W. Wei, Z. X. You, Q. Z. Yang, H. Yue, Z. G. Su and G. H. Ma, *Advanced Functional Materials*, 2011, 21, 3446-3453.
2. E. N. Cline, M. H. Li, S. K. Choi, J. F. Herbstman, N. Kaul, E. Meyhöfer, G. Skiniotis, J. R. Baker, R. G. Larson and N. G. Walter, *Biomacromolecules*, 2013, 14, 654-664.
3. F. Danhier, B. Vroman, N. Lecouturier, N. Crokart, V. Pourcelle, H. Freichels, C. Jérôme, J. Marchand-Brynaert, O. Feron and V. Préat, *J. Controlled Release*, 2009, 140, 166-173.

4. R. T. Liggins and H. M. Burt, *International journal of pharmaceutics*, 2004, 282, 61-71.

5. K. M. Huh, H. S. Min, S. C. Lee, H. J. Lee, S. Kim and K. Park, *Journal of Controlled Release*, 2008, 126, 122-129.

6. Z. Wei, J. Hao, S. Yuan, Y. Li, W. Juan, X. Sha and X. Fang, *International journal of pharmaceutics*, 2009, 376, 176-185.

7. A. M. Harmon, M. H. Lash, S. M. Sparks and K. E. Uhrich, *Journal of Controlled Release*, 2011, 153, 233-239.

8. M. V. Lozano, D. Torrecilla, D. Torres, A. Vidal, F. Domínguez and M. J. Alonso, *Biomacromolecules*, 2008, 9, 2186-2193.

9. D. Du, N. Chang, S. Sun, M. Li, H. Yu, M. Liu, X. Liu, G. Wang, H. Li and X. Liu, *J. Controlled Release*, 2014, 182, 99-110.

10. M. Li, H. Yu, T. Wang, N. Chang, J. Zhang, D. Du, M. Liu, S. Sun, R. Wang and H. Tao, *Journal of Materials Chemistry B*, 2014, 2, 1619-1625.

11. Z. Zhang and S. S. Feng, *Biomaterials*, 2006, 27, 4025-4033.

12. L. Mu and S. Feng, *Journal of controlled release*, 2003, 86, 33-48.

13. M. Li, H. Deng, H. Peng and Q. Wang, *Journal of nanoscience and nanotechnology*, 2014, 14, 415-432.

14. F. Song, X. Li, Q. Wang, L. Liao and C. Zhang, *Journal of Biomedical Nanotechnology*, 2015, 11, 40-52.

15. H. Peng, X. Liu, R. Wang, F. Jia, L. Dong and Q. Wang, *Journal of Materials Chemistry B*, 2014, 2, 6435-6461.

16. J. Fang, H. Nakamura and H. Maeda, *Advanced drug delivery reviews*, 2011, 63, 136-151.

17. F. Jia, X. Liu, L. Li, S. Mallapragada, B. Narasimhan and Q. Wang, *J. Controlled Release*, 2013, 172, 1020-1034.

18. I. I. Slowing, C. W. Wu, J. L. Vivero-Escoto and V. S. Y. Lin, *Small*, 2009, 5, 57-62.

19. W. J. Song, J. Z. Du, T. M. Sun, P. Z. Zhang and J. Wang, *Small*, 2010, 6, 239-246.

20. L. Wei, J. Tang, Z. Zhang, Y. Chen, G. Zhou and T. Xi, *Biomedical Materials*, 2010, 5, 044103.

21. H. Xu, Q. Jiang, N. Reddy and Y. Yang, *J. Mater. Chem.*, 2011, 21, 18227.

22. Y. Yang, S. Wang, Y. Wang, X. Wang, Q. Wang and M. Chen, *Biotechnol. Adv.*, 2014, 32, 1301-1316.

23. F. Ding, H. Deng, Y. Du, X. Shi and Q. Wang, *Nanoscale*, 2014, 6, 9477-9493.

24. A. O. Elzoghby, W. M. Samy and N. A. Elgindy, *Journal of Controlled Release*, 2012, 157, 168-182.

25. E. J. Lee, S. A. Khan, J. K. Park and K. H. Lim, *Bioprocess Biosystems Eng.*, 2012, 35, 297-307.

26. X. Zhen, X. Wang, C. Xie, W. Wu and X. Jiang, *Biomaterials*, 2013, 34, 1372-1382.

27. L. Chen, G. E. Remondetto and M. Subirade, *Trends in Food Science & Technology*, 2006, 17, 272-283.

28. J. Xie, Y. Cao, M. Xia, X. Gao, M. Qin, J. Wei and W. Wang, *Advanced healthcare materials*, 2013, 2, 795-799.

29. S. Lee, N. S. A. Alwahab and Z. M. Moazzam, *International journal of pharmaceutics*, 2013, 454, 388-393.

30. H. J. Wang, Z. X. Lin, X. M. Liu, S. Y. Sheng and J. Y. Wang, *J. Controlled Release*, 2005, 105, 120-131.

31. L. Muthuselvi and A. Dhathathreyan, *Colloids Surf. B. Biointerfaces*, 2006, 51, 39-43.

32. Q. Zhong, H. Tian and S. Zivanovic, *J. Food Process. Preserv.*, 2009, 33, 255-270.

33. A. Patel, Y. Hu, J. K. Tiwari and K. P. Velikov, *Soft Matter*, 2010, 6, 6192.

34. X. Liu, Q. Sun, H. Wang, L. Zhang and J. Y. Wang, *Biomaterials*, 2005, 26, 109-115.

35. S. Podaralla, R. Averineni, M. Alqahtani and O. Perumal, *Molecular pharmaceutics*, 2012, 9, 2778-2786.

36. Y. Luo, Z. Teng and Q. Wang, *Journal of agricultural and food chemistry*, 2012, 60, 836-843.

37. Y. Luo, T. T. Wang, Z. Teng, P. Chen, J. Sun and Q. Wang, *Food chemistry*, 2013, 139, 224-230.

38. M. J. Ernsting, W. D. Foltz, E. Undzys, T. Tagami and S. D. Li, *Biomaterials*, 2012, 33, 3931-3941.

39. K. Zhu, T. Ye, J. Liu, Z. Peng, S. Xu, J. Lei, H. Deng and B. Li, *International*

journal of pharmaceutics, 2013, 441, 721-727.

40. K. Zhu, T. Ye, J. Liu, Z. Peng, S. Xu, J. Lei, H. Deng and B. Li, *Int. J. Pharm.*, 2013, 441, 721-727.

41. L. He, H. Liang, L. Lin, B. R. Shah, Y. Li, Y. Chen and B. Li, *Colloids Surf. B. Biointerfaces*, 2015, 126, 288-296.

42. Y. Luo, Z. Teng, T. T. Wang and Q. Wang, *J. Agric. Food. Chem.*, 2013, 61, 7621-7629.

43. Y. Luo, Z. Teng and Q. Wang, *J. Agric. Food. Chem.*, 2012, 60, 836-843.

44. S. Kenth, J. P. Sylvestre, K. Fuhrmann, M. Meunier and J. C. Leroux, *Journal of pharmaceutical sciences*, 2011, 100, 1022-1030.

45. Q. Hu, X. Gao, T. Kang, X. Feng, D. Jiang, Y. Tu, Q. Song, L. Yao, X. Jiang and H. Chen, *Biomaterials*, 2013, 34, 9496-9508.

46. Q. Hu, G. Gu, Z. Liu, M. Jiang, T. Kang, D. Miao, Y. Tu, Z. Pang, Q. Song and L. Yao, *Biomaterials*, 2013, 34, 1135-1145.

47. F. P. Seib, G. T. Jones, J. Rnjak-Kovacina, Y. Lin and D. L. Kaplan, *Advanced healthcare materials*, 2013, 2, 1606-1611.

48. W. Trickler, A. Nagvekar and A. Dash, *Pharmaceutical research*, 2009, 26, 1963-1973.

49. J. Yao, L. Zhang, J. Zhou, H. Liu and Q. Zhang, *Mol. Pharm.*, 2013, 10, 1080-1091.

50. C. Yang, Y. Liu, Y. He, Y. Du, W. Wang, X. Shi and F. Gao, *Biomaterials*, 2013, 34, 6829-6838.

51. I. Rivkin, K. Cohen, J. Koffler, D. Melikhov, D. Peer and R. Margalit, *Biomaterials*, 2010, 31, 7106-7114.

52. L. Lin, W. Xu, H. Liang, L. He, S. Liu, Y. Li, B. Li and Y. Chen, *Colloids Surf. B. Biointerfaces*, 2015.

53. W. P. Su, F. Y. Cheng, D. B. Shieh, C. S. Yeh and W. C. Su, *International journal of nanomedicine*, 2012, 7, 4269.

573 **Graphical Abstract**

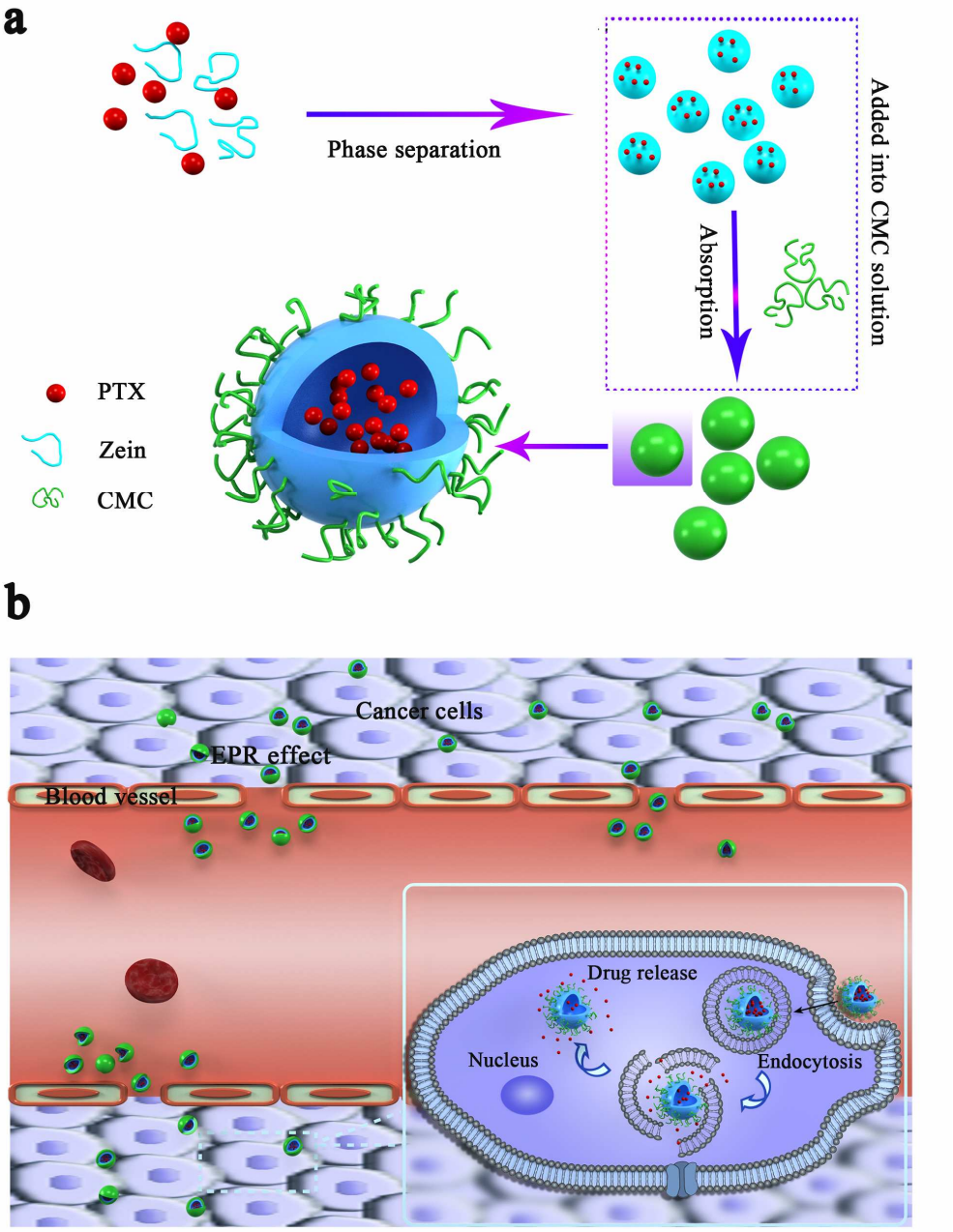

574

575

576

577

578

579

580 **Table 1**

581 Optimization of PTX-loaded zein-CMC NPs.

Samples	Size(nm)	PDI	Zeta potential(mV)	EE(%)
Z/CMC 2:1	188.4±2.9	0.39±0.05	-50.1±0.92	72.5±1.55
Z/CMC 1:1	178.2±4.2	0.26±0.01	-52.7±0.51	89.4±0.74
Z/CMC 1:2	189.8±2.5	0.24±0.00	-52.3±0.51	89.9±0.25
Z/CMC 1:3	189.1±0.5	0.27±0.01	-54.4±1.36	95.5±0.20
Z/CMC 1:4	196.7±2.9	0.34±0.01	-55.7±0.59	94.6±0.37

582 Samples represent formulations with different mass ratios of zein-CMC with the concentration of
583 PTX at 50μg ml^{-1}. PDI, polydispersity. EE(%),encapsulation efficiency. Data displayed as mean±
584 SD(n=3).
585
586
587
588
589
590
591
592
593
594
595
596
597
598
599

Figure captions:

Hongshan Liang, Huazhong Agriculture University.

Figure 1. SEM images of zein-CMC NPs at zein : CMC ratio of 1:3 w/w (a) and (b). TEM image, size distribution and optical photograph of zein-CMC NPs at zein : CMC ratio of 1:3 w/w (c). TEM image, size distribution and optical photograph of zein-CMC NPs at zein : CMC ratio of 1:3 w/w after refrigerated for 30 days (d). TEM image, size distribution and optical photograph of the PTX-loaded zein-CMC NPs at zein : CMC ratio of 1:3 w/w at PTX concentration of 80 μg ml^{-1} (e). TEM images, size distribution and optical photograph of PTX-loaded zein-CMC NPs at zein : CMC ratio of 1:3 w/w in PTX concentration of 80 μg ml^{-1}after refrigerated for 30 days (f).

Figure 2. Concentrations in μg ml^{-1} are the final content in the suspension. Zein-CMC NPs were prepared at zein : CMC ratio of 1:3 w/w (a). In vitro release profiles of free PTX and PTX from zein-CMC NPs prepared at zein:CMC ratio of 1 : 3 w/w in PTX concentration of 80μg ml^{-1} in PBS buffers (pH 7.4) over 72h at 37 ℃ (b). EE(%),encapsulation efficiency; LC(%), loading capacity . Data displayed as mean±SD (n=3)

Figure 3. Cellular uptake of NPs: CLSM images of intracellular uptake of courmarin-labeled PTX-NPs by sensitive HepG2 cells (a) and resistant MCF-7 cells (b). Cells were counter-stained with DAPI (for nuclei) and LysoTracker Red (for lysosomes). The scale bars represent 20μm.

Figure 4. Flow cytometry results of HepG2 and MCF-7 cells as founction of time treated with the courmarin 6-labeled PTX-NPs (a), (b) and (c). Data displayed as mean±SD (n=3). * $p < 0.05$; ** $p < 0.01$; *** $p < 0.001$; versus the control group.

Figure 5. In vitro cytotoxicity of the NPs, PTX and PTX-loaded NPs against PTX sensitive and resistant tumor cells: HeLa cells incubated for 24 h (a) or 48 h (b), HepG2 cells incubated for 24 h (c) or 48h (d), MCF-7 cells incubated for 24 h (e) or 48 h (f) and A549 cells incubated for 24 h (g) or 48 (h). In all panels, the indicated concentrations are PTX doses. It should be noted that for evaluating PTX-loaded NPs, equal concentrations of blank NPs were employed to eliminate the effect of vehicles in MTT assay. Data displayed as mean±SD (n=6). * $p < 0.05$; ** $p < 0.01$; *** $p < 0.001$; versus the PTX group.

Figure 6. The apoptosis assay on sensitive HepG2 cells and resistant MCF-7 cells after treatment with the NPs, PTX and PTX-loaded NPs for 24h (a).The PTX concentration was 8μg mL^{-1} in all cells. (b)reflects the proportion of apoptotic and necrotic cells after the NPs, PTX and PTX-loaded NPs treatment. Data displayed as mean±SD (n=3). * $p < 0.05$; ** $p < 0.01$; *** $p < 0.001$; versus the control group.

Figure 7. CLSM images showing HepG2 cells (a) and MCF-7 cells (b) with immunofluorescence stained of tubulin after treatment with PTX or PTX-loaded NPs for 24 h or 48 h. The dose of PTX was 1.0 and 8.0μg mL^{-1} for HepG2 and MCF-7

cells, respectively. The scale bars represent 20 μm.

Scheme 1. Schematic illustration of the process of preparing PTX-loaded NPs by phase separation (a). Schematic representation of the mechanisms by which nanocarrier can deliver PTX to tumor tissues. Passive targeting is achieved by extravasation of NPs through enhanced permeability of the tumor vasculature (EPR effect) (b).

667 **Figure 1.**

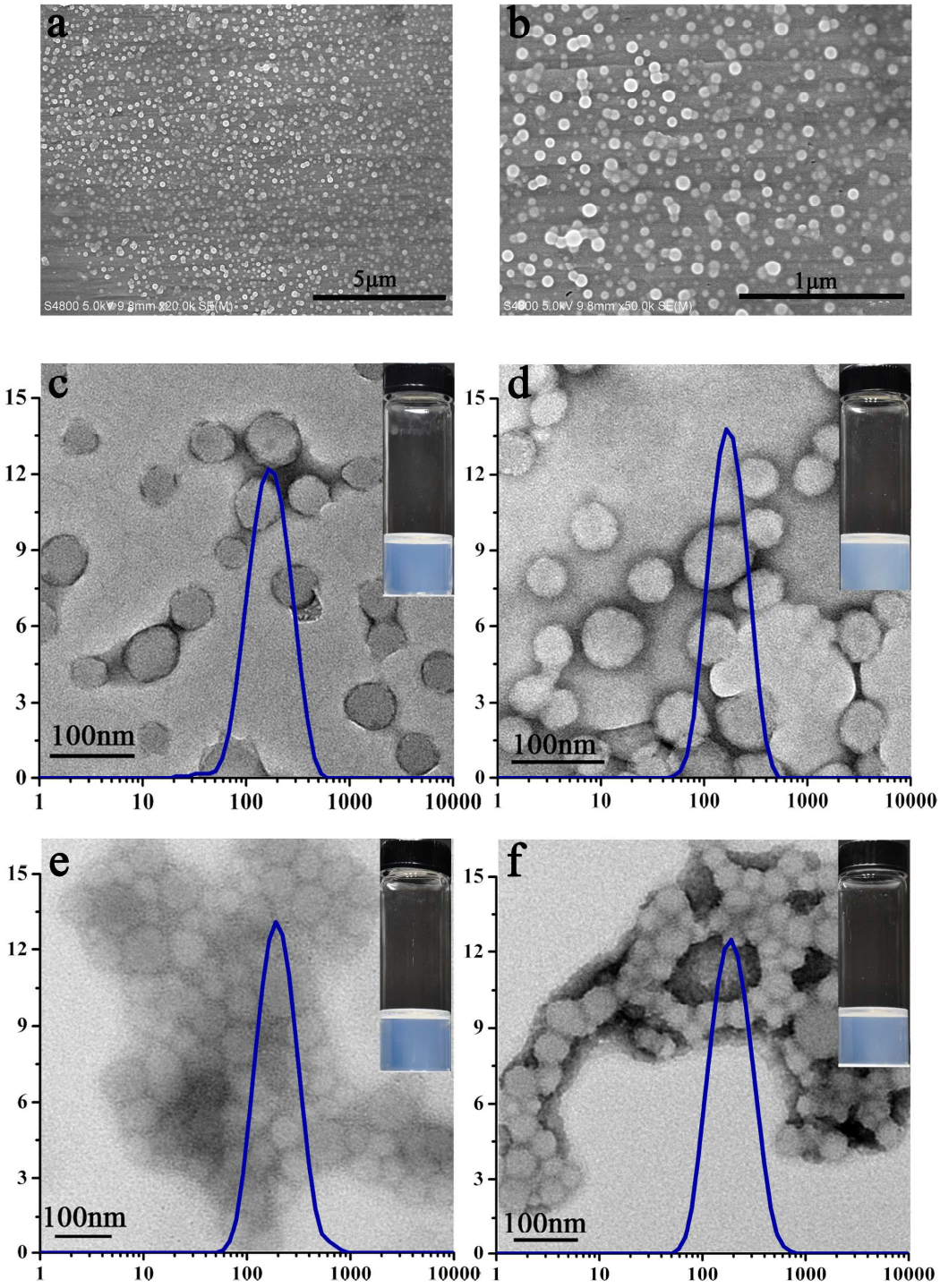

668

669

670

671

672 **Figure 2.**

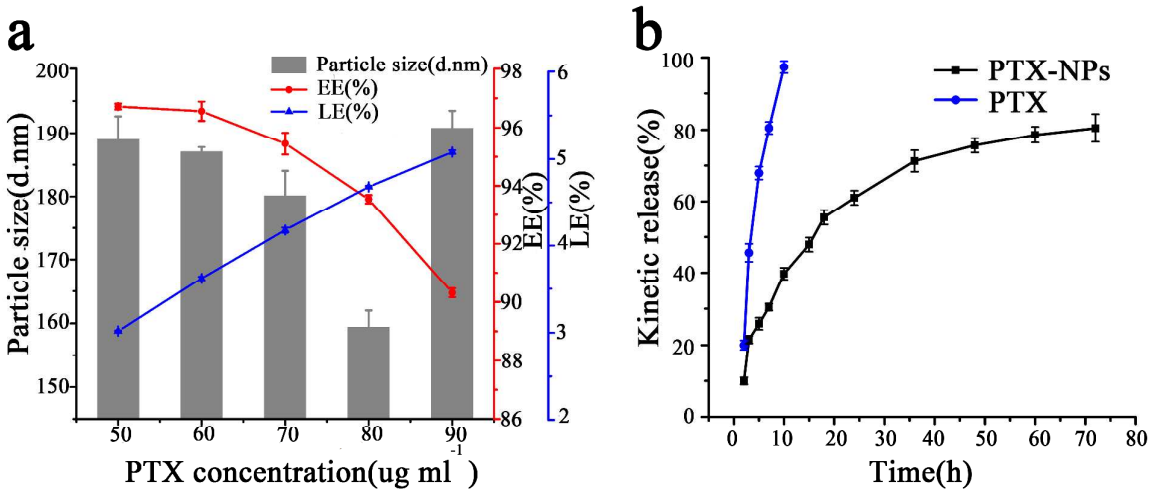

673

674

675

676

677

678

679

680

681

682

683

684

685

686

687

688

689 **Figure 3.**

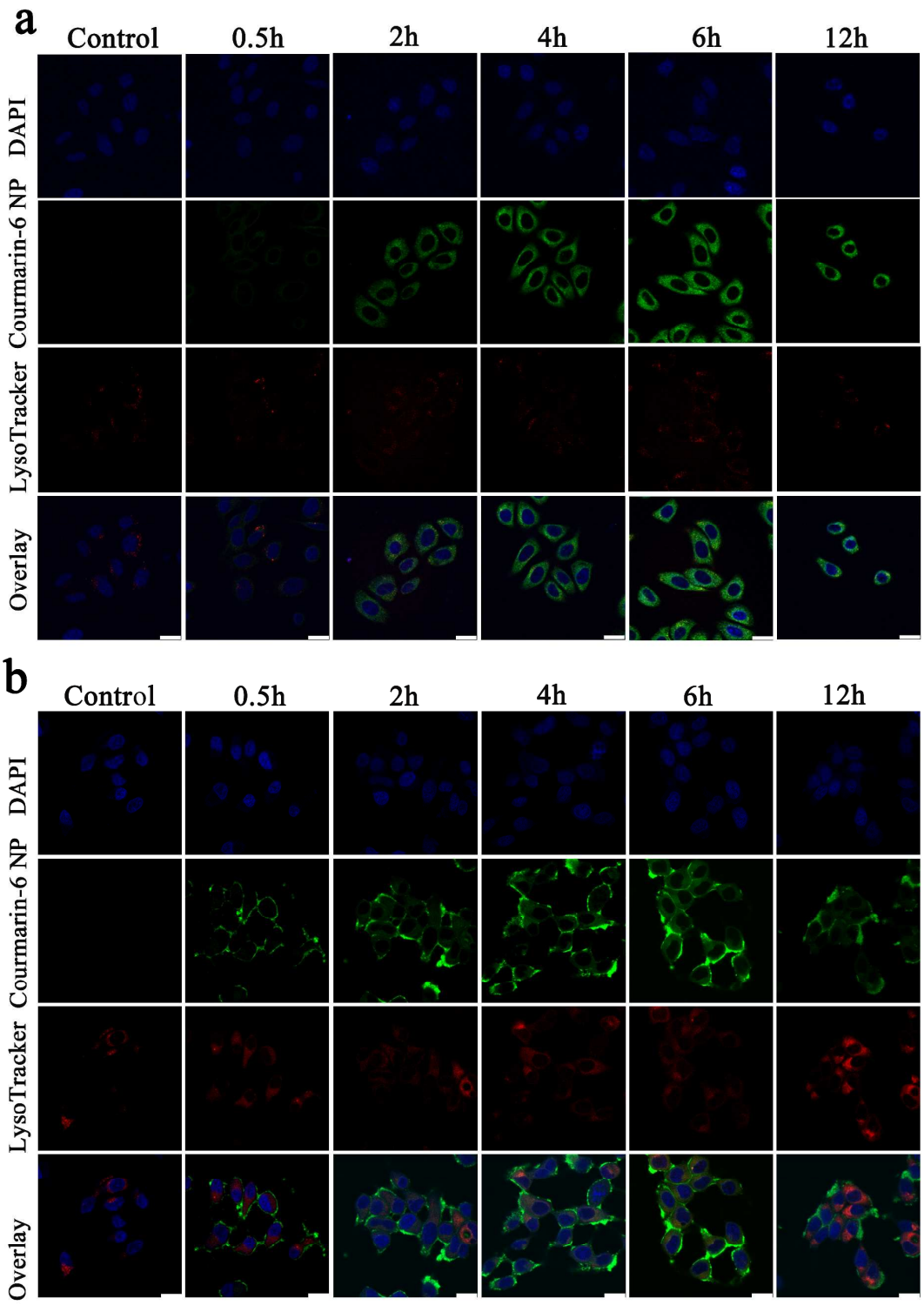

690

691

692

693 **Figure 4.**

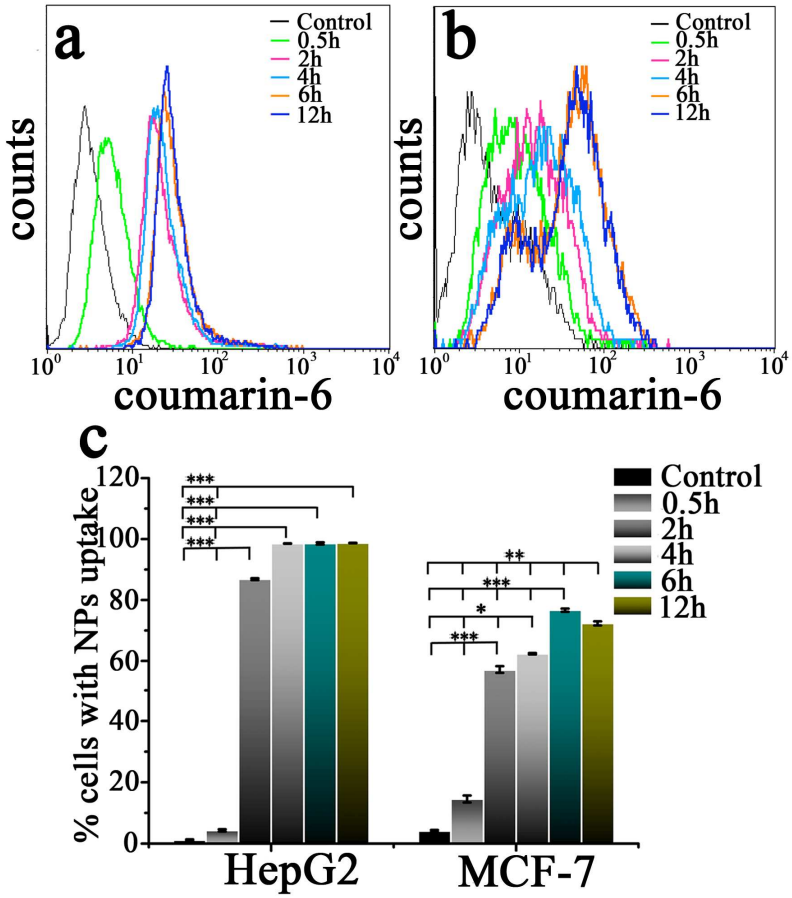

694

695

696

697

698

699

700

701

702

703

704

Figure 5.

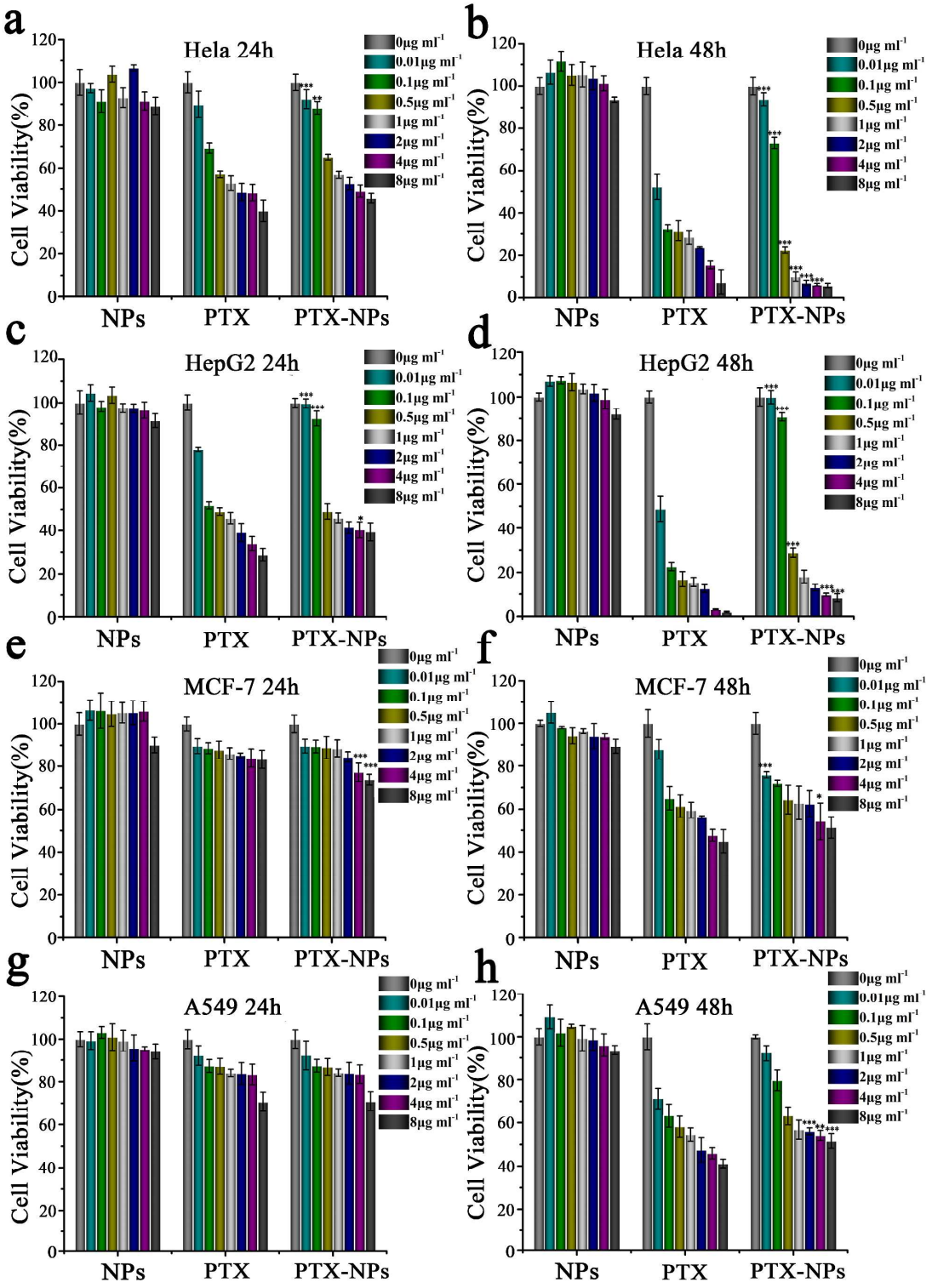

709 **Figure 6.**

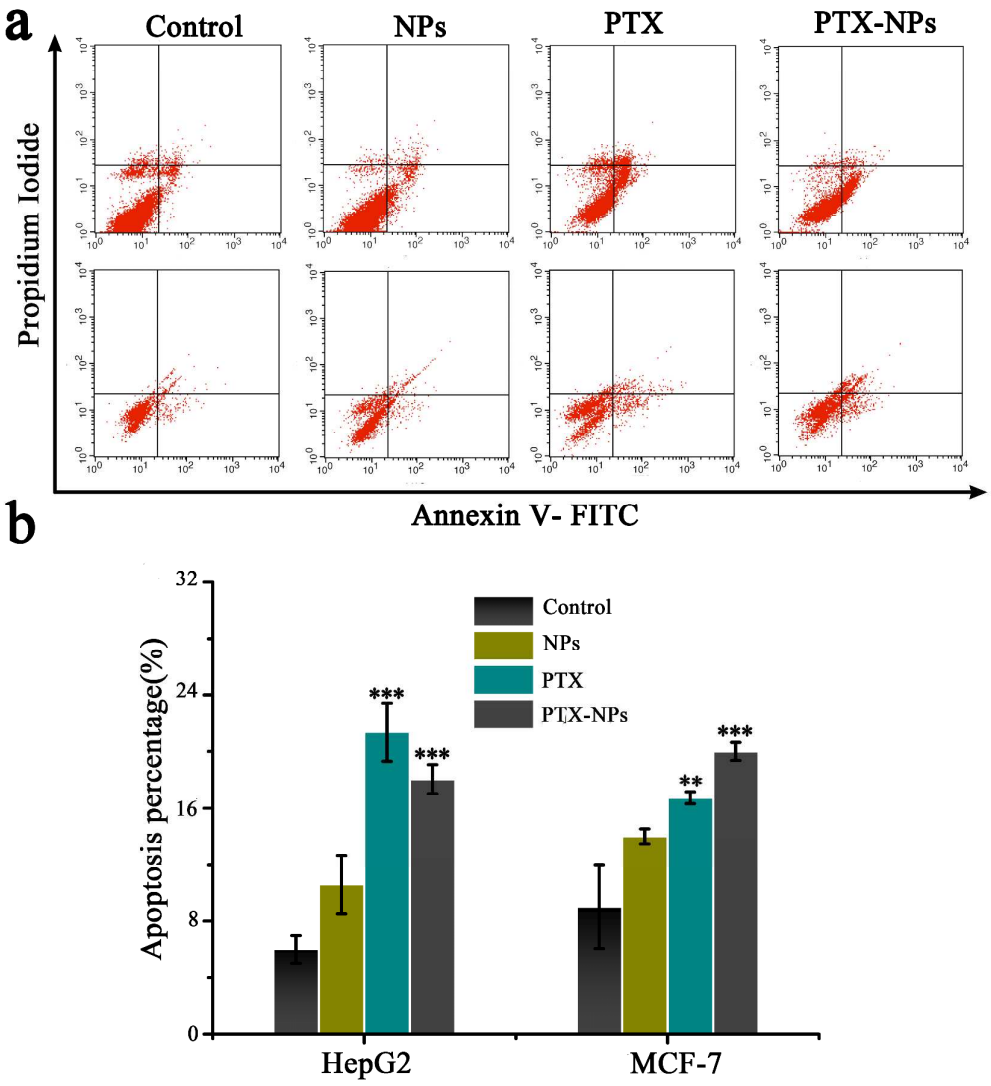

710

711

712

713

714

715

716

717

718 **Figure 7.**

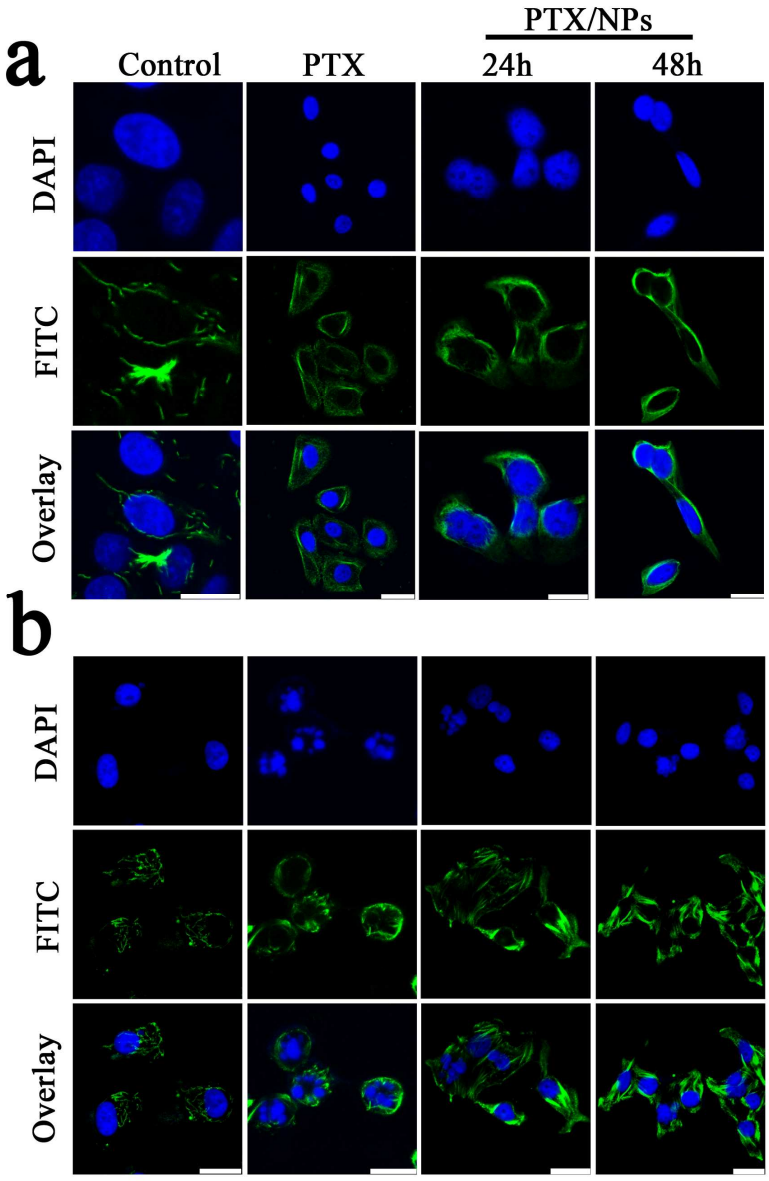

719

720

721

722

723

724

725

726 **Scheme 1.**

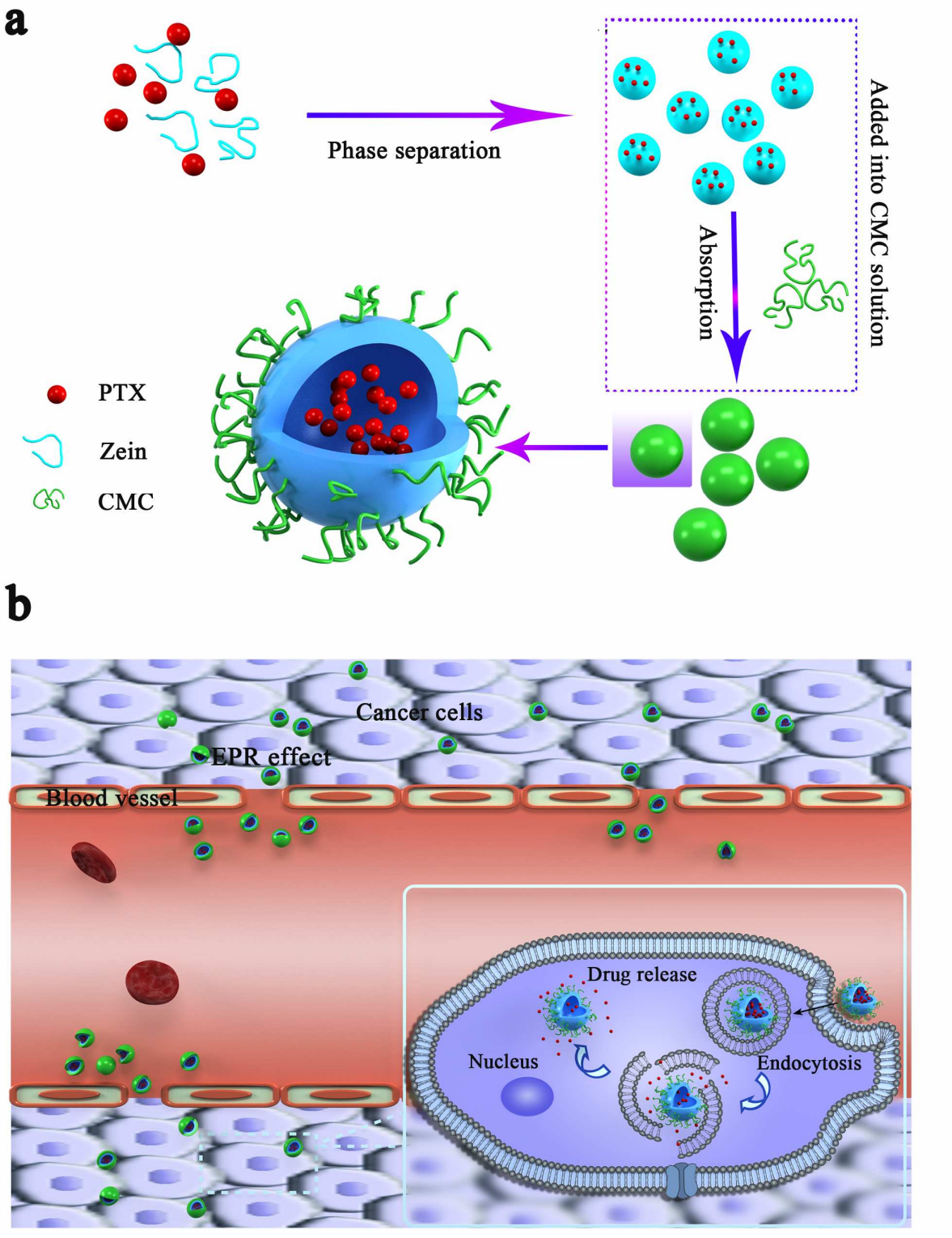

727

728

729